JOURNAL OF THERMOPHYSICS AND HEAT TRANSFER
Vol. 23, No. 4, October–December 2009

Heat Flux Duplication Between Ground Facility and Hypersonic Flight

P. F. Barbante*
Politecnico di Milano, 20133 Milano, Italy

DOI: 10.2514/1.35808

The development of reentry space vehicles requires a precise qualification of their thermal protection system materials. The material catalytic properties should be determined for test conditions relevant to the real flight mission program. However, perfect reproduction of the flight environment in a ground facility is practically impossible for reacting flows and one is obliged to resort to a partial simulation. In an attempt to overcome such an issue, we present a methodology that allows establishing under which hypothesis and approximations the flowfield inside a ground facility is equivalent, regarding the heat flux load, to the real flowfield experienced by a space vehicle. The analytical results of the theory are compared with numerical predictions and agree favorably with them.

Nomenclature

c	=	mass fraction
$\mathcal{D}_{ij}$	=	binary diffusion coefficient between species i and j, m^2/s
f	=	Blasius function
g	=	$h_0/h_{0\delta}$, nondimensional mixture total enthalpy
h	=	enthalpy, J/kg
h_0	=	$h + \frac{1}{2}u^2$, total enthalpy, J/kg
k_b	=	Boltzmann constant
k_w	=	wall catalytic speed, m/s
Le	=	Lewis number
l_0	=	$\rho\mu/\rho_\delta\mu_\delta$, Chapman–Rubesin parameter
M	=	Mach number
M^M	=	mixture molar mass, kg/mol
M_i^M	=	molar mass of species i, kg/mol
m	=	mass of particle, kg
Ns	=	number of species in the mixture
Pr	=	Prandtl number
p	=	pressure, Pa
q	=	heat flux, W/m^2
r	=	distance from body axis, m
R	=	body nose radius, m
$\mathcal{R}$	=	universal gas constant, J/(mol K)
R_g	=	specific gas constant, J/(kg K)
T	=	mixture temperature, K
u, v	=	tangential and normal velocity components, m/s
$\dot{w}$	=	mass chemical production rate, $kg/(m^3 s)$
x, y	=	Cartesian coordinates, m
x_i	=	mole fraction of species i
γ	=	wall catalytic recombination probability
η	=	transformed y coordinate
θ	=	mixture nondimensional temperature
μ	=	mixture viscosity, m^2/s
ξ	=	transformed x coordinate
ρ	=	mixture density, kg/m^3

Subscripts

A	=	atoms
M	=	molecules
s	=	stagnation point
w	=	wall surface
δ	=	boundary-layer outer edge
∞	=	freestream

Superscripts

f	=	flight
t	=	ground facility

Received 22 November 2007; revision received 9 June 2009; accepted for publication 14 June 2009.

*Researcher, Department of Mathematics, Piazza Leonardo da Vinci 32; paolo.barbante@polimi.it.

I. Introduction

THE determination of the catalytic properties of thermal protection system (TPS) materials is crucial for the design of an optimal flight strategy of aerospace vehicles: as a matter of fact, the heat flux for a fully catalytic wall can be more than twice the heat flux for a noncatalytic wall. Furthermore, TPS material catalytic behavior can be influenced by the local gas temperature, pressure, and chemical composition [1]. This situation requires ground facilities that are able to provide representative testing conditions for the evaluation of the material performances, because TPS materials should be tested in real flight conditions, to safely rely on their catalytic properties. However, for reacting flows, the wide range of real flight conditions cannot be fully reproduced in the existing experimental ground facilities [2,3]. The usual strategy to overcome such a problem is to resort to some kind of partial simulation: only some characteristics of the flight environment, which are of interest in the specific experiment, are reproduced.

In this contribution, we present a methodology that allows establishing which hypothesis and approximations make the flowfield inside a plasma wind tunnel able to reproduce the real flowfield experienced by a specific part of a reentry vehicle. The focus is on heat flux duplication between flight and ground facility. In [4] we presented a methodology for local heat flux duplication in the stagnation region; here, we extend the previous work to the whole boundary layer downstream of the stagnation point.

II. Local Heat Flux Duplication Concept

In this section, we derive an analytical expression for wall heat flux that will be used to establish the conditions needed for heat flux duplication between real flight and wind tunnel.

We suppose that a boundary layer exists and the flow is laminar, two-dimensional, or axisymmetric and made of Ns chemically reacting perfect-gas species. These assumptions exclude fully three-dimensional or turbulent flows, but are consistent with the goal of deriving an approximate analytical solution of boundary-layer equations, which is subsequently used to establish the heat flux duplication criteria.

However, even if boundary-layer equations are simpler than Navier–Stokes equations, it is still impossible to determine a general analytical solution, and therefore additional simplifying assumptions are needed.

The Lees–Dorodnitsyn coordinate transformation [5,6] is applied to the boundary-layer equations; the new independent variables are defined as

$$\xi = \int_0^x \rho_\delta \mu_\delta u_\delta r^{2\epsilon}\, \mathrm{d}x$$

(which plays the role of a transformed streamwise coordinate) and

$$\eta = \frac{u_\delta r^\epsilon}{\sqrt{2\xi}} \int_0^y \rho\, \mathrm{d}y$$

(which plays the role of a transformed normal to the wall coordinate), where $\epsilon = 1$ for axisymmetric flows and $\epsilon = 0$ for two-dimensional flows. We also assume that the mixture of Ns reacting species can be reduced to a suitable binary mixture made of atoms and diatomic molecules: such an approximation has been shown to be satisfactory for air [7,8] and has the practical task of making the analytical solution of the boundary-layer equations more straightforward. However, the former assumption is not mandatory, and the present approach can be extended to mixtures with three or more components [8].

The boundary layer is assumed to be locally self-similar; that is, all the terms in the boundary-layer equations, except β (to be defined later), that contain derivatives with respect to the ξ variables are negligible compared with terms that contain derivatives with respect to the η variable [6]. This approximation, although not valid in general, is still acceptable for the purpose of computing the heat flux load [9]. The simplified and transformed boundary-layer equations (the continuity equation is automatically taken into account in the present formulation) finally read as follows.

Species continuity equation:

$$f\frac{\partial c_A}{\partial \eta} + \frac{\partial}{\partial \eta}\left(l_0 \frac{Le}{Pr}\frac{\partial c_A}{\partial \eta}\right) = -\frac{2\xi}{\rho_\delta \mu_\delta u_\delta^2 r^{2\epsilon}}\frac{\dot{w}_A}{\rho} \tag{1}$$

where $\dot{w}_A$ is the production-destruction term [5] of atoms by means of gas-phase chemical reactions taking place inside the boundary layer; for our binary mixture, the only possible reactions are the dissociation of diatomic molecules into atoms and the opposite recombination process. The expression of $\dot{w}_A$ is determined by the law of mass action [10] and reads

$$\frac{\dot{w}_A}{\rho} = k_b \frac{2p_\delta}{\mathcal{R}T}\left(K_c \frac{1-c_A}{2} - \frac{2p_\delta}{\mathcal{R}T}\frac{c_A^2}{1+c_A}\right) \tag{2}$$

The chemical equilibrium constant K_c is computed by means of statistical thermodynamics [11], and the reaction rate k_b for atom recombination has the form [12] $k_b = A_b T^{\eta_b}$. Inserting the expression of k_b in Eq. (2) and writing the temperature as $T = \theta T_\delta$, the production term $\dot{w}_A$ now reads

$$\frac{\dot{w}_A}{\rho} = \frac{\bar{w}_A}{\tau_c} = \frac{2p_\delta}{\mathcal{R}} A_b T_\delta^{\eta_b - 1}\theta^{\eta_b - 1}\left(K_c \frac{1-c_A}{2} - \frac{2p_\delta}{\mathcal{R}T_\delta}\frac{c_A^2}{1+c_A}\right) \tag{3}$$

where τ_c is a typical time of gas-phase chemical reactions; it depends on the reaction rate constant A_b, from boundary-layer pressure p_δ and temperature T_δ at the boundary-layer edge. Its expression reads

$$\tau_c = \frac{\mathcal{R}}{2p_\delta A_b T_\delta^{\eta_b - 1}} \tag{4}$$

Momentum equation:

$$f\frac{\partial}{\partial \eta}\left(\frac{\partial f}{\partial \eta}\right) + \frac{\partial}{\partial \eta}\left[l_0 \frac{\partial}{\partial \eta}\left(\frac{\partial f}{\partial \eta}\right)\right] = \beta\left[\left(\frac{\partial f}{\partial \eta}\right)^2 - \frac{\rho_\delta}{\rho}\right] \tag{5}$$

The nondimensional boundary-layer tangential velocity is given by $u/u_\delta = \partial f/\partial \eta$. The term β reads

$$\beta = \frac{2\xi}{u_\delta}\frac{\mathrm{d}u_\delta}{\mathrm{d}\xi} = -\frac{2\xi}{\rho_\delta u_\delta^2}\frac{\mathrm{d}p_\delta}{\mathrm{d}\xi} \tag{6}$$

and is due to the effect of external pressure gradient.

Total enthalpy equation:

$$f\frac{\partial g}{\partial \eta} + \frac{\partial}{\partial \eta}\left(\frac{l_0}{Pr}\frac{\partial g}{\partial \eta}\right) = -\frac{u_\delta^2}{2h_{0\delta}}\frac{\partial}{\partial \eta}\left[\frac{l_0}{Pr}(Pr-1)\frac{\partial}{\partial \eta}\left(\frac{\partial f}{\partial \eta}\right)^2\right] - \frac{\partial}{\partial \eta}\left[\frac{l_0}{Pr}(Le-1)\frac{\partial c_A}{\partial \eta}\frac{h_A - h_M}{h_{0\delta}}\right] \tag{7}$$

Under the reasonable hypothesis that the Lewis number is close to 1 for a reacting mixture [9] and the wall is highly cooled, the last term on the right-hand side of Eq. (7) is neglected. The right-hand side of the momentum equation (5) can be neglected if one is interested only in the heat flux evaluation [6,9]. This assumption reduces the momentum equation to the well-known Blasius form [13] (when $l_0 = 1$ in the boundary layer) and allows analytically solving the species and energy equations if l_0, Pr, and Le are kept constant; the resulting heat flux predictions are still satisfactory for engineering purposes [9,14].

The following boundary conditions apply to Eqs. (1), (5), and (7).

Momentum equation:

$$f(0) = f_w = 0, \qquad \frac{\partial f}{\partial \eta}(0) = \left.\frac{\partial f}{\partial \eta}\right|_w = 0, \qquad \frac{\partial f}{\partial \eta}(\infty) = \left.\frac{\partial f}{\partial \eta}\right|_\delta = 1$$

Total enthalpy equation:

$$g(0) = g_w, \qquad g(\infty) = g_\delta = 1$$

Species equation:

$$\frac{\partial c_A}{\partial \eta}(0) = \left.\frac{\partial c_A}{\partial \eta}\right|_w = \frac{Prk_w}{Le\mu_w}\frac{\sqrt{2\xi}}{u_\delta r^\epsilon} c_{Aw} = E_w c_{Aw}, \qquad c_A(\infty) = c_{A\delta} \tag{8}$$

Equation (8) states that the diffusion flux at the wall is equal to the chemical-reaction rate, due to wall heterogeneous catalysis, which is computed by the simplified expression $k_w \rho_w c_{Aw}$ [15,16], where k_w is the wall catalytic speed and is linked to the wall recombination probability γ by the Hertz-Knudsen relation [16]:

$$k_w = \gamma\sqrt{\frac{k_b T_w}{2\pi m_A}}$$

where $\gamma = 0$ corresponds to a noncatalytic wall, and $\gamma = 1$ corresponds to a fully catalytic wall [16]. The factor E_w is the ratio between the wall catalytic speed k_w and a typical diffusion speed $Le\mu_w u_\delta r^\epsilon/(Pr\sqrt{2\xi})$. E_w can be interpreted as a Damköhler number [6], hereinafter called the heterogeneous Damköhler number, for wall catalysis and characterizes the relative importance of diffusion and catalysis in the determination of wall chemical composition. E_w is influenced by the quantity $u_\delta r^\epsilon/\sqrt{\xi}$, which depends on the external flowfield (and body geometry) and is therefore called the flight-condition factor f_c. We note that f_c is affected not only by the outer-flow local conditions at the boundary-layer edge but also by the outer-flow history through the transformed coordinate ξ. The physical meaning of f_c can be understood by inverting the relation between the transformed coordinate η and the original coordinate y; the maximum value of η is of order 1 [17] and the inversion gives an estimate of the boundary-layer thickness δ:

$$\delta \approx \frac{\sqrt{2}}{\rho_\delta}\frac{\sqrt{\xi}}{u_\delta r^\epsilon} = \frac{\sqrt{2}}{\rho_\delta}\frac{1}{f_c} \tag{9}$$

It is therefore evident that the flight-condition factor f_c governs the boundary-layer thickness.

With f as the known Blasius function, Eqs. (1) and (7) can be solved analytically for c_A and g and their solutions read

$$c_A(\eta) = c_{Aw} + \left.\frac{\partial c_A}{\partial \eta}\right|_w F_c(\eta) - \frac{\tau_f}{\tau_c} G(\eta) \tag{10}$$

$$g(\eta) = g_w + \left.\frac{\partial g}{\partial \eta}\right|_w F_g(\eta) + \frac{u_\delta^2}{2h_{0\delta}}(1 - Pr)H(\eta) \tag{11}$$

The quantity τ_f in Eq. (10) is a typical boundary-layer flow time and is equal to

$$\tau_f = \frac{Pr}{Le}\frac{2\xi}{\rho_\delta \mu_\delta u_\delta^2 r^{2\epsilon}} \tag{12}$$

The flight-condition factor f_c and τ_f are not independent but are linked by the relation

$$\tau_f = \frac{2Pr}{Le\rho_\delta \mu_\delta}\frac{1}{f_c^2} \tag{13}$$

We note that Eq. (10) contains the ratio of a typical flow time and a typical chemistry time (i.e., the Damköhler number for gas-phase chemical reactions).

The functions $F_c(\eta)$, $F_g(\eta)$, and $H(\eta)$ involve integrals of f and its derivatives; the function $G(\eta)$ is an integral of f and of the chemical-reaction term $\bar{w}_A$ and represents the effect of chemical reactions on the boundary-layer composition:

$$F_c(\eta) = \int_0^\eta \exp\left(-\int_0^{\eta'} \frac{Pr}{Le} f \, d\eta''\right) d\eta' \tag{14}$$

$$G(\eta) = \int_0^\eta \exp\left(-\int_0^{\eta'} \frac{Pr}{Le} f \, d\eta''\right)\left[\int_0^{\eta'} \exp\left(\int_0^{\eta''} \frac{Pr}{Le} f \, d\eta'''\right)\bar{w}_A \, d\eta''\right] d\eta' \tag{15}$$

$$F_g(\eta) = \int_0^\eta \exp\left(-\int_0^{\eta'} Prf \, d\eta''\right) d\eta' \tag{16}$$

$$H(\eta) = \int_0^\eta \exp\left(-\int_0^{\eta'} Prf \, d\eta''\right) \times \left[\int_0^{\eta'} \exp\left(\int_0^{\eta''} Prf \, d\eta'''\right)\frac{\partial^2}{\partial \eta^2}\left(\frac{\partial f}{\partial \eta}\right)^2 d\eta''\right] d\eta' \tag{17}$$

At the wall and at the boundary-layer edge, the preceding functions are equal to

$$F_c(0) = 0, \qquad G(0) = 0, \qquad F_g(0) = 0, \qquad H(0) = 0$$

$$\frac{\partial F_c}{\partial \eta}(0) = 1, \qquad \frac{\partial G}{\partial \eta}(0) = 0, \qquad \frac{\partial F_g}{\partial \eta}(0) = 1, \qquad \frac{\partial H}{\partial \eta}(0) = 0$$

$$F_c(\infty) = \frac{1}{0.47}\left(\frac{Le}{Pr}\right)^{1/3}, \qquad G(\infty) = G_\delta$$

$$F_g(\infty) = \frac{1}{0.47 Pr^{1/3}}, \qquad H(\infty) = \frac{1}{2Pr^{1/4}}$$

The exact expression of the chemical rate G_δ, which is the integral effect of gas-phase chemical reactions in the boundary layer, is not written, because the conditions needed for heat flux duplication imply equal G_δ in flight and in the ground facility, as shown at the end of this section. Application of boundary conditions provides the desired wall derivatives of c_A and g to be inserted into Eqs. (10) and (11):

$$\left.\frac{\partial c_A}{\partial \eta}\right|_w = 0.47 Pr^{1/3}\frac{E_w}{Le^{1/3}E_w + 0.47Pr^{1/3}}\left(c_{A\delta} + \frac{\tau_f}{\tau_c}G_\delta\right) \tag{18}$$

$$\left.\frac{\partial g}{\partial \eta}\right|_w = 0.47 Pr^{1/3}\left[(1 - g_w) + \frac{u_\delta^2}{4h_{0\delta}}\frac{Pr - 1}{Pr^{1/4}}\right] \tag{19}$$

The wall boundary condition for atomic species [i.e., Eq. (18)] is jointly influenced by gas-phase and heterogeneous Damköhler numbers.

The wall heat flux can now be computed:

$$q_w = \frac{\rho_\delta \mu_\delta}{Pr}\frac{u_\delta r^\epsilon}{\sqrt{2\xi}}\left[h_{0\delta}\left.\frac{\partial g}{\partial \eta}\right|_w + (Le - 1)\left.\frac{\partial c_A}{\partial \eta}\right|_w (h_{Aw} - h_{Mw})\right] \tag{20}$$

The quantity $h_{Aw} - h_{Mw}$ (difference of wall static enthalpy) can be approximated, when wall temperature is less than 2000 K, by Δh_A (i.e., the enthalpy of formation of atomic species). Substitution of the expressions for wall derivatives, given by Eqs. (18) and (19), in Eq. (20) provides, after some algebraic rearrangement, the final heat flux form:

$$q_w = 0.332\frac{\rho_\delta \mu_\delta u_\delta r^\epsilon}{Pr^{2/3}\sqrt{\xi}}(h_{0\delta} - h_{0w})\left\{1 + \frac{u_\delta^2(Pr - 1)}{4(h_{0\delta} - h_{0w})Pr^{1/4}} + \frac{Le - 1}{Le^{1/3}}\left[1 + 0.47\left(\frac{Pr}{Le}\right)^{\frac{1}{3}}\frac{1}{E_w}\right]^{-1}\frac{[c_{A\delta} + (\tau_f/\tau_c)G_\delta]\Delta h_A}{h_{0\delta} - h_{0w}}\right\} \tag{21}$$

Equation (21) states that heat flux is a function of flight-condition factor f_c, total enthalpy difference between boundary-layer outer edge and wall, recovery factor $(Pr - 1)/Pr^{1/4}$, speed, density and chemical composition at the outer edge, chemical rate G_δ in the boundary layer, gas-phase Damköhler number τ_f/τ_c, and heterogeneous Damköhler number E_w. Duplication of all the preceding quantities between flight and ground facility would ensure the desired heat flux similarity. Equal total enthalpy and chemical composition at the boundary-layer edge and equal gas-phase Damköhler number imply that the chemical-reaction behavior is the same and therefore the chemical rate G_δ is also identical. It is interesting to observe that the gas-phase Damköhler number is function of the gas-phase chemical time τ_c and of the flight-condition factor f_c [see Eq. (13)]; heterogeneous Damköhler number is a function of wall catalycity k_w and of the flight-condition factor f_c [see Eq. (8)]. We note again that wall catalytic behavior is affected by the f_c factor and this confirms our statement that TPS materials should be tested for real flight conditions. It is clear from the preceding discussion that the heat flux depends not only on the local conditions at the boundary-layer outer edge but also on the factor f_c that governs the boundary-layer thickness and takes into account the external flowfield history by means of the transformed coordinate ξ. Therefore, heat flux is correctly duplicated in the ground facility if the local boundary-layer structure is also duplicated in the facility; it is the purpose of the Results section to provide some examples of how this can be achieved. The test cases to be presented (stagnation point, flat plate, and half-sphere) are for real reacting air mixtures, and the computations are performed without any of the simplifying assumptions used to derive Eq. (21); the flowfield is laminar for all test cases.

III. Numerical Method

The computations in the stagnation point of the wind-tunnel sample and on the flat plate are made with a boundary-layer code [5]. The governing equations are discretized with Hermitian fourth-order-accurate polynomials. The remaining computations are done by means of a Navier–Stokes finite volume code for reacting flows [18,19]. The finite volume convective terms are discretized with the hybrid upwind splitting Riemann solver [20]; a MUSCL- type reconstruction [21] is applied to achieve second-order accuracy: van Albada's limiter is used in the present work. The transport terms

(stress tensor, heat, and diffusion fluxes) are centrally discretized with second-order accuracy.

The two codes make use of the same set of physicochemical models, thus allowing for a coherent and physically consistent comparison between the two series of computations [22]. Diffusion fluxes are computed by means of the exact Stefan–Maxwell equations [23,24] instead of the simplified and inconsistent Fick's law that is often found in literature. This choice is important if one wants to correctly compute the heat flux [23,24], and it is therefore necessary to assess the correctness of the present theory.

The implementation of the wall boundary conditions for the reacting species equations [Eq. (8) for the equivalent binary mixture] is performed by means of the Stefan–Maxwell equations; to the author's best knowledge, this approach has never appeared before in literature. It is based on the observation that, at the wall, the diffusion flux of the species is known, because it is equal to the catalytic heterogeneous reaction rate $\dot{w}_{i,\mathrm{cat}}$. In such a way, the unknown at the wall is no longer the diffusion flux, but the wall gradient $\partial x_i/\partial n$ of chemical composition. The modified Stefan–Maxwell equations at the wall read

$$\frac{M^M}{\rho}\sum_{j=1}^{Ns}\left(\frac{x_i\dot{w}_{j,\mathrm{cat}}}{M_j^M\mathcal{D}_{ij}}-\frac{x_j\dot{w}_{i,\mathrm{cat}}}{M_i^M\mathcal{D}_{ij}}\right)=\frac{\partial x_i}{\partial n} \tag{22}$$

The main advantage of this implementation is that the boundary condition is fully consistent with the diffusion flux computation in the interior of the domain and ensures the correct coupling of wall chemistry and diffusion.

The accuracy of computations of both codes has been checked by means of grid refinement. For the boundary-layer code, 100 points in the direction across the boundary layer are taken; if the number of grid points is doubled, the computed heat flux changes by less than 0.5%. For all the Navier–Stokes code computations, doubling the number of cells varies the heat flux by less than 3%.

IV. Results

A. Stagnation Point

At the stagnation point of a body, Eq. (21) reduces to (for a two-dimensional body, there is a factor of 0.47 instead of 0.664)

$$\begin{aligned}q_w=&\frac{0.664}{Pr^{2/3}}\sqrt{\rho_\delta\mu_\delta}\sqrt{\frac{\mathrm{d}u_{\delta s}}{\mathrm{d}x}}(h_{0\delta}-h_{0w})\\&\times\left\{1+\frac{Le-1}{Le^{1/3}}\left[1+\frac{0.664}{\sqrt{\rho_\delta\mu_\delta}}\left(\frac{Le}{Pr}\right)^{2/3}\sqrt{\frac{\mathrm{d}u_{\delta s}}{\mathrm{d}x}}\frac{\mu_w}{k_w}\right]^{-1}\right.\\&\left.\times\frac{[c_{A\delta}+(\tau_f/\tau_c)G_\delta]\Delta h_A}{h_{0\delta}-h_{0w}}\right\}\end{aligned} \tag{23}$$

The quantity $\mathrm{d}u_{\delta s}/\mathrm{d}x$ is the external flowfield velocity gradient at the stagnation point. The f_c factor is proportional to $(\mathrm{d}u_{\delta s}/\mathrm{d}x)^{1/2}$, and τ_f is equal to $a(\mathrm{d}u_{\delta s}/\mathrm{d}x)^{-1}Pr/Le$, where $a=1/2$ for axisymmetric flow and $a=2$ for two-dimensional flow. Stagnation-point heat flux is a function of velocity gradient, total enthalpy (which, at the stagnation point, coincides with static enthalpy), density and chemical composition at the boundary-layer outer edge, and wall enthalpy and catalycity. As a consequence, when these quantities are the same in the wind tunnel and in flight, the heat flux is equal for the two cases (same G_δ is implied by the previous conditions, because the gas-phase Damköhler number is identical). Density can be replaced by pressure, because density is a unique function of enthalpy, chemical composition, and pressure. When the flow is close to chemical equilibrium at the boundary-layer edge (a not uncommon condition in the stagnation region), chemical composition is a function only of enthalpy and pressure, and the heat flux in the stagnation region is the same in flight and in the wind tunnel if enthalpy, pressure, and velocity gradient are the same at the outer edge of the boundary layer [4,25].

To validate the preceding statements, we establish the stagnation-point heat flux duplication between a TPS sample of 50 mm in diameter placed inside the von Karman Institute high-enthalpy subsonic Plasmatron wind tunnel [26] and a real vehicle. The flowfield at the stagnation point of the wind-tunnel sample is computed with the boundary-layer code, and the flowfield over the real body is computed with the Navier–Stokes code.

The values of total enthalpy, pressure, and velocity gradient at the stagnation point of the sample are [27] $h_{0\delta}=22.3$ MJ/kg, $p_\delta=10,020$ Pa, and $\mathrm{d}u_\delta/\mathrm{d}x=3902$ s^{-1}. The details of the mixed experimental numerical procedure used to obtain the previous stagnation-point values are provided in [27]. In agreement with the cited methodology [27], local chemical equilibrium is assumed at the outer edge of the sample boundary layer.

The extrapolation method of [4] allows determining the geometry and the freestream flying conditions of the corresponding vehicle in such a way to ensure the same stagnation parameters for the vehicle as in the wind tunnel. The vehicle has a nose radius of 0.68 m and flies at an altitude of 62.5 km and at a Mach number $M=21.4$. The reacting mixture chosen for the computations is five-species air. The wall temperature is taken to be 1500 K and the wall reactions due to catalycity are $\mathrm{N}+\mathrm{N}\rightarrow\mathrm{N}_2$ and $\mathrm{O}+\mathrm{O}\rightarrow\mathrm{O}_2$.

Figure 1 shows the stagnation-point heat flux for the full range of wall catalycity values; the heat flux value for $\gamma=0$ is not shown because of the logarithmic scale, but it is practically equal to that for $\gamma=10^{-4}$. Computed heat flux difference between Navier–Stokes and the boundary layer goes from 1% for the noncatalytic wall to 7% for the fully catalytic wall. The main reason of such a good agreement is that equal enthalpy, pressure, and velocity gradient ensure that the same boundary-layer structure is present on the sample and the vehicle, although the dimensions of the two objects are considerably different. Stagnation-point boundary-layer thickness is a function of the square root of the inverse of velocity gradient [13] [see also Eq. (9)] and, as shown in Figs. 2 and 3, is almost identical for the sample and the vehicle. Velocity gradient also dictates the typical flow time τ_f at the stagnation point, which is the same for both configurations. Enthalpy and pressure are also the same at the boundary-layer edge, and therefore the characteristic chemical time τ_c is also the same. Therefore, the gas-phase Damköhler number is equal for both wind tunnel and flight, and chemical composition inside the boundary layer should be close for ground facility and flight. The heterogeneous Damköhler number, which is governed by wall catalytic speed k_w and flight-condition factor f_c, is the same. Equations (10) and (18) predict that the boundary-layer chemical composition is a function of the gas-phase and heterogeneous Damköhler numbers; because they are the same in the wind tunnel and in flight, a close agreement in chemical composition has to be expected.

The preceding statements are validated by the profiles of oxygen and nitrogen shown in Fig. 2. Oxygen is fully dissociated at the boundary-layer outer edge and remains fully dissociated all along the boundary layer; agreement between ground and flight profiles is

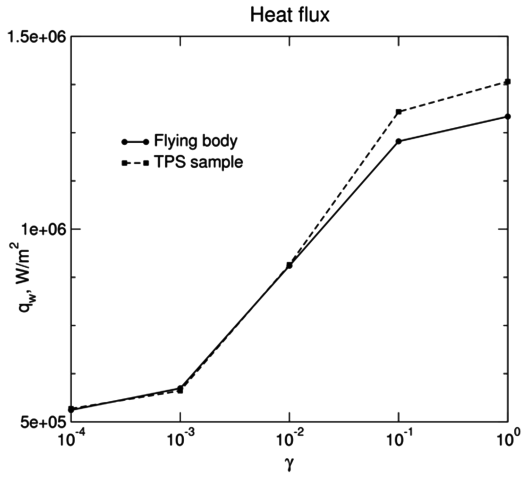

Fig. 1 Stagnation heat flux for different catalycity levels.

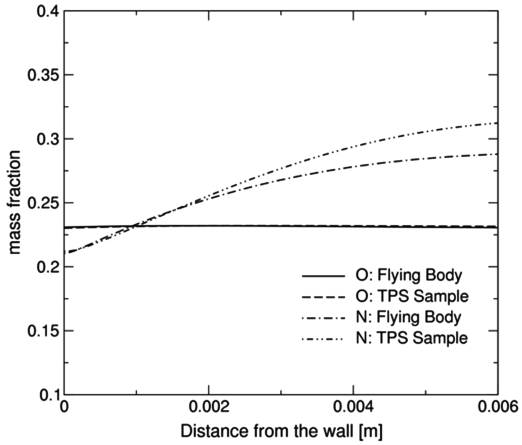

Fig. 2 Stagnation streamline O and N mass fractions for a noncatalytic wall.

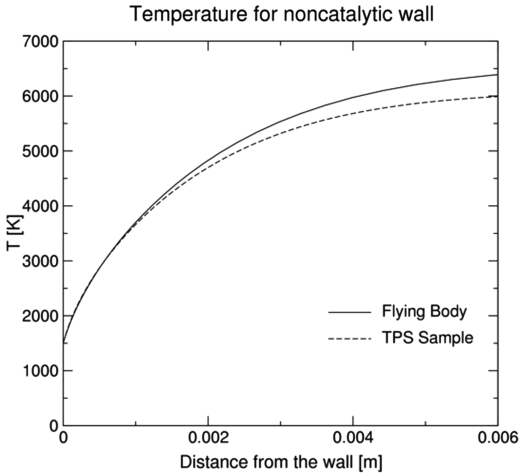

Fig. 3 Stagnation streamline temperature for a noncatalytic wall.

excellent. Nitrogen is partially dissociated at the boundary-layer edge and recombines inside the boundary layer. The flow, as already mentioned, is assumed to be at chemical equilibrium at the boundary-layer edge of the wind-tunnel sample [26], but it is in weak nonequilibrium for the vehicle; however, the details of nitrogen behavior close to the wall are almost identical. This discrepancy in chemical composition violates, in principle, one of the hypotheses needed for heat flux similarity, but in this specific case, its effect on heat flux and wall chemical composition is negligible.

The temperature profile is shown in Fig. 3; the agreement is excellent (in particular, close to the wall), thus proving the validity of the present theory.

B. Flat Plate

The flight-condition factor $f_c = u_\delta r^\epsilon / \sqrt{\xi}$ reduces for a flat plate to $\sqrt{u_\delta / x}$, under the hypothesis that boundary-layer outer-edge conditions are constant. It should be noted that $\tau_f \approx x/u_\delta$ and therefore same f_c implies the same boundary-layer thickness [see Eq. (9)] and typical flow time [see Eq. (13)].

Flat-plate heat flux is a function of total enthalpy, velocity, density, and chemical composition at the boundary-layer outer edge; of gas-phase chemistry time τ_c, u_δ/x (which has the dimensions of a velocity gradient); and of the wall enthalpy and catalycity. Therefore, the heat flux is equal in flight and in the ground facility if the previous quantities are the same in both cases. As in the stagnation-point case, equal enthalpy, chemical composition and u_δ/x accounts for the correct duplication of gas-phase Damköhler number and of chemical rate G_δ; the heterogeneous Damköhler number is also duplicated. Unfortunately, equal outer-edge velocity implies equal flat-plate dimensions, because u_δ/x has to be the same. However, it is possible to relax the condition on velocity and to allow for different dimensions in flight and in the wind tunnel by imposing the same outer-edge static enthalpy instead of the total enthalpy. This assumption has an effect on heat flux prediction, as discussed in the remainder of the section.

To assess our statements, the boundary layer along a flat plate is computed with the boundary-layer code. The outer-edge boundary conditions are as follows: $p_\delta = 12,525$ Pa, $T_\delta = 6000$ K, and $M_\delta = 0.1,\ 0.3,\ 0.9,\ 2$. The outer-edge chemical composition is considered to be the equilibrium composition. The wall is assumed to be at radiative equilibrium, and the emissivity coefficient is set equal to 0.85; wall catalytic chemical reactions are $N + N \rightarrow N_2$ and $O + O \rightarrow O_2$. The reacting mixture is five-species air, and the computations are made for two levels of catalytic recombination probability: $\gamma = 0$ and 1.

In Figs. 4 and 5, the heat flux for the noncatalytic wall and fully catalytic wall, respectively, is shown for all Mach numbers. The heat flux is plotted against the normalized coordinate $x(u_{\delta,M_\delta=0.1}/u_\delta)$, which is the same for the whole Mach number range. Suppose that we want to simulate the real flight flow with a Mach 0.1 wind-tunnel flow; the agreement in heat flux (except for a small region near the flat-plate tip, in which the classical boundary-layer theory is not adequate) ranges from excellent for $M_\delta = 0.1$, 0.3, and 0.9 to acceptable for $M_\delta = 2$. The maximum heat flux difference for a noncatalytic wall is around 21% between $M_\delta = 0.1$ and 2, for a fully catalytic wall, it is around 18–19% for the same Mach number range.

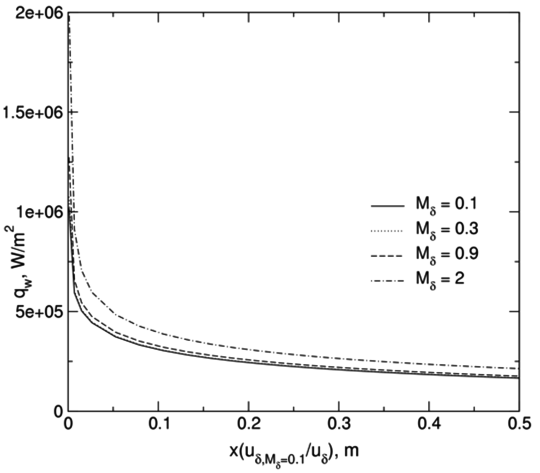

Fig. 4 Flat-plate heat flux: noncatalytic wall.

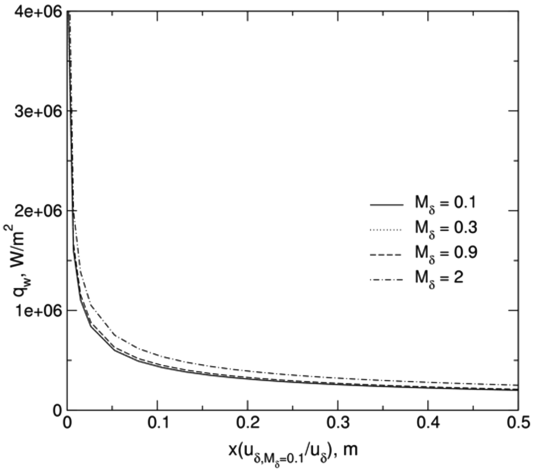

Fig. 5 Flat-plate heat flux: fully catalytic wall.

The heat flux difference is easily explained: it is due to the viscous dissipation inside the boundary layer that naturally increases with Mach number. Although the outer-edge Mach number is different, the structure of the boundary layer is similar for equal values of the normalized coordinate $x(u_{\delta,M_\delta=0.1}/u_\delta)$ for all cases. Atomic oxygen and nitrogen profiles are shown in Fig. 6 for a noncatalytic wall. Only the profiles for $M_\delta = 0.1$ and 2 are shown; those for the remaining Mach numbers fall between the two. The agreement is good and the boundary-layer thickness is the same: in effect, the same u_δ/x implies the same gas-phase and heterogeneous Damköhler numbers and the same boundary-layer thickness [13]. The temperature profile for a noncatalytic wall is shown in Fig. 7; the agreement is good, and the profile for $M = 2$ has a slightly higher temperature because of viscous dissipation.

C. Half-Sphere

We want to explore the possibility of simulating the heat flux over the whole spherical front nose of a reentry vehicle with a spherical probe inside a low-Mach-number high-temperature wind tunnel, such as, for example, the von Karman Institute Plasmatron [26].

Inspection of Eq. (21) shows that the key parameters for heat flux similitude are total enthalpy, velocity, and chemical composition at the boundary-layer outer edge, wall enthalpy and catalycity, and the flight-condition factor $f_c = u_\delta r^\epsilon/\sqrt{\xi}$, which governs gas-phase and heterogeneous Damköhler numbers. The f_c factor can be computed analytically for both configurations; in effect, the ξ coordinate can be rewritten as

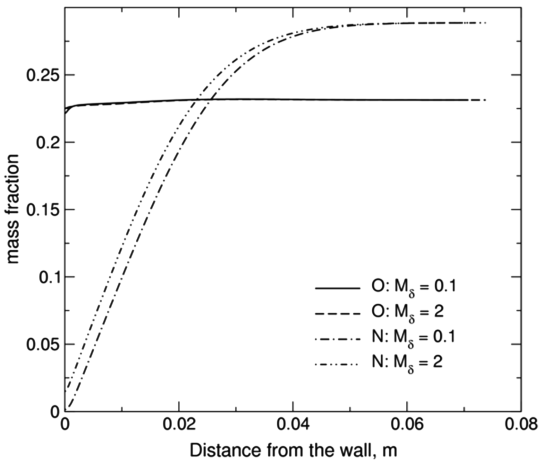

Fig. 6 Flat-plate O and N mass fraction at $x(u_{\delta,M_\delta=0.1}/u_\delta) = 0.5$ for a noncatalytic wall.

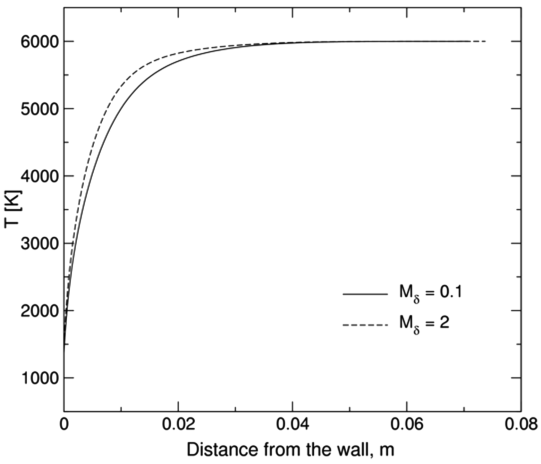

Fig. 7 Flat-plate temperature at $x(u_{\delta,M_\delta=0.1}/u_\delta) = 0.5$ for a noncatalytic wall.

$$\xi \approx \omega_{\delta s} \int_0^x p_\delta u_\delta r^{2\epsilon}\,\mathrm{d}x$$

where $\omega_\delta = p_\delta/(R_{g,\delta}T_\delta)$ is almost constant over the whole boundary-layer edge and has been taken equal to its stagnation-point value.

For the reentry vehicle, which flies at hypersonic Mach number, pressure p_δ is given by the modified hypersonic Newtonian law [28]; velocity u_δ is, with good accuracy, equal to [9] $(\mathrm{d}u_{\delta s}/\mathrm{d}x)x$; and x is the boundary-layer streamwise coordinate. The expression of f_c for the hypersonic flow over the spherical nose of a reentry vehicle reads

$$f_c^f \approx \frac{1}{\sqrt{\rho_{\delta s}\mu_{\delta s}}}\sqrt{\frac{\mathrm{d}u_{\delta s}}{\mathrm{d}x}}\left[2 - \left(\frac{13}{9} - \frac{3}{4\gamma_\infty M_\infty^2}\right)\frac{x^2}{R^2} + \left(\frac{13}{60} + \frac{1}{9\gamma_\infty M_\infty^2} - \frac{1}{3\gamma_\infty^2 M_\infty^4}\right)\frac{x^4}{R^4}\right] \tag{24}$$

where γ_∞ and M_∞ are the specific heat ratio and Mach number of the freestream, respectively.

The Mach number inside the von Karman Institute Plasmatron is in the range 0.05–0.4 [26,27]; at these regimes, the plasma flow of dissociated air behaves as an incompressible flow. It is therefore reasonable to suppose that outside the boundary layer, the velocity and pressure distributions over the front half of the spherical probe itself are given by the standard potential flow theory [29]; however, the latter assumption is valid only if the ground-facility plasma jet is uniform; irrotational; and without radial gradients in velocity, enthalpy, and chemical composition (a condition that is not always satisfied [30] in the real ground facility). The velocity, predicted by potential theory, at the sample boundary-layer edge is [29] $u_\delta = 3/2u_\infty \sin(x/R)$, where u_∞ is the freestream velocity, R is the spherical probe radius, x is the boundary-layer streamwise coordinate, and the pressure p_δ is computed with the Bernoulli equation [29]. The expression of f_c for the probe reads

$$f_c^t \approx \frac{1}{\sqrt{\rho_{\delta s}\mu_{\delta s}}}\sqrt{\frac{\mathrm{d}u_{\delta s}}{\mathrm{d}x}}\left[2 - \left(\frac{1}{3} + \frac{3}{2}\gamma_\infty M_\infty^2\right)\frac{x^2}{R^2} + \left(\frac{1}{144} + \frac{25}{32}\gamma_\infty M_\infty^2 - \frac{27}{64}\gamma_\infty^2 M_\infty^4\right)\frac{x^4}{R^4}\right] \tag{25}$$

The velocity gradient at the probe stagnation point is equal to [29] $3u_\infty/(2R)$; γ_∞ is the specific heat ratio, and M_∞ is the Mach number of the plasma jet impinging on the probe.

Equations (24) and (25) show that even if all the remaining similarity parameters are equal, heat flux is, in general, different for the two configurations, because f_c^f and f_c^t (with related flow time, boundary-layer thickness, and Damköhler numbers) are different. More precisely, setting equal stagnation-point velocity gradients, the heat flux is quite close for $x/R \le 0.3$, where the contributions to f_c factor of terms containing x^2/R^2 and x^4/R^4 are negligible. Outside of this region, Eqs. (24) and (25) predict a wind-tunnel f_c factor and heat flux higher than those of the flight.

The flight freestream conditions and body geometry are chosen as altitude 61 km, Mach number 21.5, nose radius 1.79 m, and stagnation-point velocity gradient 1502 s^{-1}; for the wind tunnel, we choose $M_\infty = 0.05$ and 0.15 (which are, for example, in the range of typical freestream Mach numbers of the von Karman Institute Plasmatron wind tunnel [27]). The corresponding probe radii (computed imposing same stagnation velocity gradient in flight and in the wind tunnel) are, respectively, $R = 10$ and 30 cm. The wind-tunnel plasma jet, as mentioned in the derivation of Eq. (25), is supposed to be uniform, with a temperature of the order of 6085 K and a pressure of 12,300 Pa; its chemical composition is the equilibrium composition [26,27]. The jet values are chosen so that the stagnation enthalpy and pressure of the probe match those of the vehicle. Vehicle and probe walls are supposed to be in radiative equilibrium, and the emissivity coefficient is set equal to 0.9; wall chemical reactions are the same as the stagnation-point test case. The reacting mixture is five-species air; computations are performed with the Navier–Stokes code.

In Fig. 8, the heat flux numerically computed for a noncatalytic radiative equilibrium wall is shown. At the stagnation point, the agreement is excellent, as should be expected because we impose identical conditions. There is practically no difference in heat flux between $M_\infty = 0.05$ and 0.15; the contribution of kinetic energy total enthalpy and therefore to heat flux is negligible. Outside of the stagnation point, the heat flux over the probe is higher than the heat flux over the real vehicle. Agreement is still good for $x/R \leq 0.3$, where wind-tunnel and flight heat fluxes differ by no more than 10%. For $x/R \leq 0.7$, probe heat flux drops to a bit more than 90% of the stagnation value and vehicle heat flux drops to 60% of the stagnation value. Outside of this range, probe heat flux is much higher than vehicle heat flux; for $x/R = \pi/2$, the former drops to roughly 60% of the stagnation-point value, whereas the latter drops to approximately 10% of the stagnation value. It is important to note that these results agree with the predictions of Eqs. (24) and (25).

Heat flux behavior is mainly influenced by the f_c factor, which is different for flight and wind tunnel, except close to the stagnation region, in which it is equal for both configurations (we recall that stagnation-point velocity gradient is forced to be equal in flight and ground facility). This is demonstrated in Fig. 9, which shows the normalized heat flux (heat flux divided by stagnation-point heat flux), which practically coincides with $f_c/(2\mathrm{d}u_{\delta s}/\mathrm{d}x)$. We note a good agreement between numerical normalized heat flux and the approximate analytical heat flux [Eqs. (24) and (25)], especially for the low-Mach-number case. It is a remarkable demonstration of the validity of the present approach, even with all the assumptions made to obtain an analytical expression for f_c and the wall heat flux.

Temperature and species profiles (atomic oxygen and nitrogen) on the stagnation streamline for flight and ground facility are shown in Figs. 10 and 11, respectively; The probe results are for $M = 0.05$; those for $M = 0.15$ are almost identical. The agreement is excellent for temperature and the boundary-layer thickness is identical. Also species profiles are in good agreement, with a small difference in the wall value of atomic nitrogen; we point out that boundary-layer thickness is well duplicated.

The temperature profile at $x/R = 0.7$ is shown in Fig. 12. The temperature value at the boundary-layer outer edge is higher for the probe. This is not surprising, because the wind-tunnel jet has a uniform temperature and chemical composition, whereas the flow behind the bow shock wave is not uniform, because the bow shock is curved. The boundary layer on the vehicle is thicker than that on the probe, and this is already implied by the value of f_c; in effect, as shown by Eq. (9), f_c is proportional to the inverse of boundary-layer thickness. Equations (24) and (25) and Fig. 9 imply that $f_c^f(0.7) \leq f_c^t(0.7)$ and therefore that the boundary layer is thicker over the vehicle.

The results just presented for the half-sphere show the strong influence of the f_c factor on the heat flux distribution when the wall is noncatalytic; Eq. (21) predicts that f_c also has a strong influence for a catalytic wall. To validate such a prediction, computations have been performed for a wall with catalytic recombination probability $\gamma = 10^{-2}$. The wall reactions are $\mathrm{N} + \mathrm{N} \rightarrow \mathrm{N}_2$ and $\mathrm{O} + \mathrm{O} \rightarrow \mathrm{O}_2$. In this specific case, the stagnation-point heat flux is 730 kW/m^2 for $M = 0.05$, 705 kW/m^2 for $M = 0.15$, and 694 kW/m^2 for $M = 21.5$, against 400 kW/m^2 for the noncatalytic wall (as shown

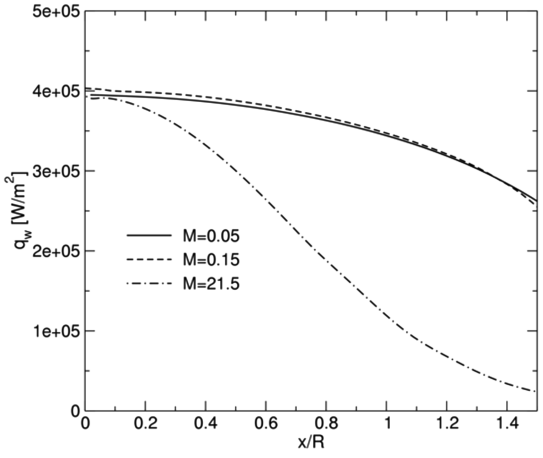

Fig. 8 Half-sphere heat flux for a radiative equilibrium noncatalytic wall.

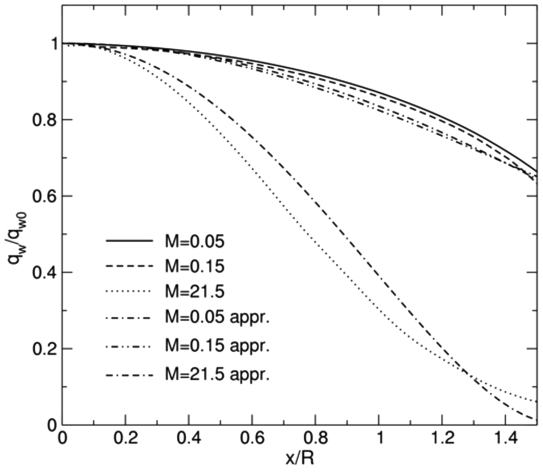

Fig. 9 Half-sphere normalized heat flux for a radiative equilibrium noncatalytic wall.

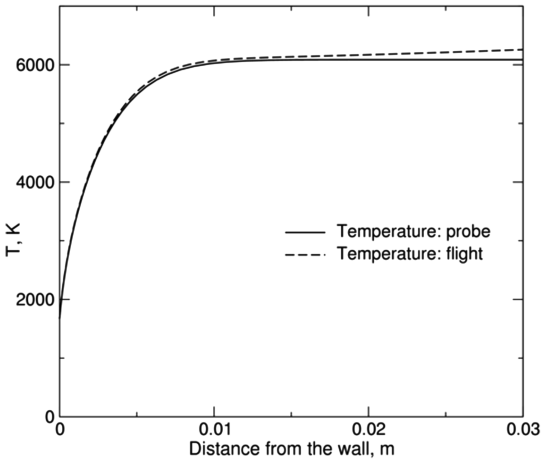

Fig. 10 Half-sphere stagnation streamline: temperature.

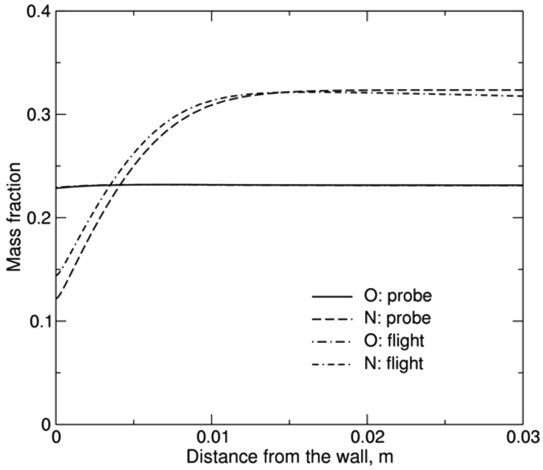

Fig. 11 Half-sphere stagnation streamline: chemical composition.

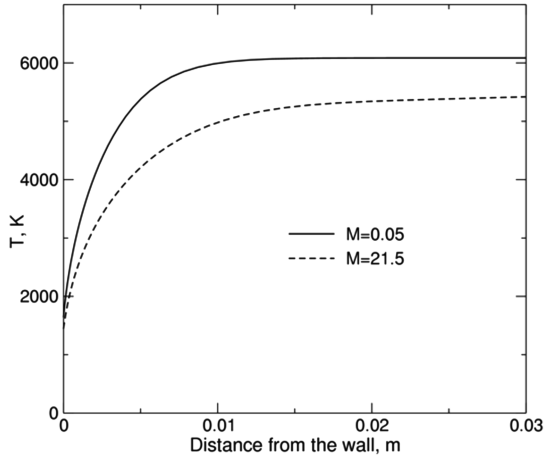

Fig. 12 Half-sphere $x/R = 0.7$: temperature for a noncatalytic wall.

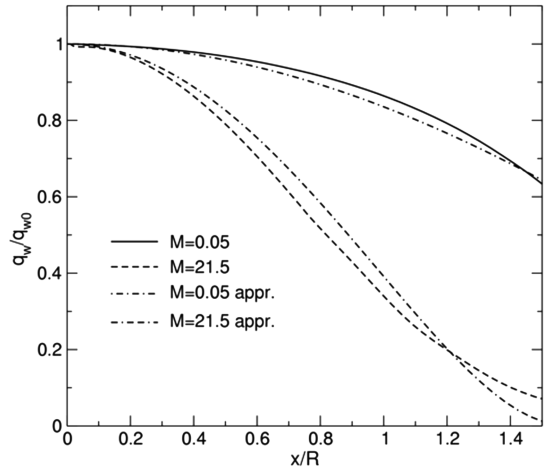

Fig. 13 Half-sphere normalized heat flux for a radiative equilibrium catalytic wall.

in Fig. 8), thus demonstrating the important effect of wall catalysis. The normalized heat flux for $\gamma = 10^{-2}$ is shown in Fig. 13; there is a good agreement between the numerical normalized heat flux and the analytical heat flux [given by Eqs. (24) and (25)], and this also demonstrates the strong influence of f_c on heat flux for a catalytic wall.

V. Conclusions

The local heat flux duplication concept, which determines the conditions for heat flux scaling between real flight and wind tunnel, has been presented with its application to three different configurations: stagnation point, flat plate, and half-sphere. As a general rule, the heat flux is correctly duplicated if the local boundary-layer structure is the same in flight and in the ground facility.

In the stagnation configuration, the equality of stagnation enthalpy, pressure, and velocity gradient is necessary for a correct reproduction of the flight thermochemical environment inside the ground facility. Results show a good agreement between flight and ground facility for all values of wall catalycity.

For the flat-plate configuration, the heat flux is not duplicated as accurately as in the stagnation-point configuration, unless the flat-plate dimensions are exactly retained. However, gas-phase and heterogeneous Damköhler numbers and flight-condition factor are well duplicated, and therefore the chemical composition in the boundary layer and the wall heterogeneous chemical-reaction phenomena are also correctly reproduced.

In the half-sphere case, as predicted by the analytical formula, the wind-tunnel heat flux is higher than the flight heat flux; the main reason is the different pressure-velocity distribution for the two cases, which affects the flight-condition factor f_c, one of the key parameters for heat flux duplication.

In all test cases, there is a good agreement between our approximate analytical formulas, with related duplication criteria, and the numerical computations for the whole range of wall catalycity values.

References

[1] Thomel, J., Lukkien, J., and Chazot, O., "A Multiscale Approach for Building a Mechanism based Catalysis Model for High Enthalpy CO_2 Flow," AIAA Paper 2007-13, 2007.

[2] Sarma, G. S. R., "Physico-Chemical Modelling in Hypersonic Flow Simulation," *Progress in Aerospace Sciences*, Vol. 36, Nos. 3–4, 2000, pp. 281–349. doi:10.1016/S0376-0421(00)00004-X

[3] Bertin, J. J., *Hypersonic Aerothermodynamics*, AIAA, Washington, 1994, Chap. 4.

[4] Barbante, P. F., and Chazot, O., "Extrapolation of Plasma Wind Tunnel Stagnation Region Flowfield," *Journal of Thermophysics and Heat Transfer*, Vol. 20, No. 3, 2006, pp. 493–499. doi:10.2514/1.17185

[5] Barbante, P. F., Degrez, G., and Sarma, G. S. R., "Computation of Nonequilibirum High-Temperature Axisymmetric Boundary-Layer Flows," *Journal of Thermophysics and Heat Transfer*, Vol. 16, No. 4, 2002, pp. 490–497. doi:10.2514/2.6723

[6] Lees, L., "Laminar Heat Transfer over Blunt-nosed Bodies at Hypersonic Flight Speeds," *Jet Propulsion*, Vol. 26, No. 4, 1956, pp. 259–269.

[7] Fay, J. A., and Riddell, F. R., "Theory of Stagnation Point Heat Transfer in Dissociating Air," *Journal of the Aeronautical Sciences*, Vol. 25, No. 2, 1958, pp. 73–85.

[8] Inger, G. R., "Highly Nonequilibrium Boundary Layer Flows of a Multicomponent Dissociated Gas Mixture," *International Journal of Heat and Mass Transfer*, Vol. 7, No. 11, 1964, pp. 1151–1774. doi:10.1016/0017-9310(64)90058-4

[9] Chung, P. M., "Chemically Reacting Nonequilibrium Boundary Layers," *Advances in Heat Transfer*, Vol. 2, No. 1, 1965, pp. 109–270.

[10] Anderson, J. D., *Hypersonic and High Temperature Gas Dynamics*, McGraw–Hill, New York, 1989, Chap. 13.

[11] Vincenti, W. G., and Kruger, C. H., *Introduction to Physical Gas Dynamics*, Wiley, New York, 1965, Chap. 4.

[12] Gupta, R. N., Yos, J. M., Thompson, R. A., and Lee, K. P., "A Review of Reaction Rates and Thermodynamic and Transport Properties for an 11-Species Air Model for Chemical and Thermal Nonequilibrium Calculations to 30000 K," NASA RP 1232, Aug. 1990.

[13] White, F. M., *Viscous Fluid Flows*, 2nd ed., McGraw–Hill, New York, 1991, Chap. 3.

[14] Inger, G. R., "Nonequilibrium Stagnation Point Boundary Layers with Arbitrary Surface Catalycity," *AIAA Journal*, Vol. 1, No. 8, 1963, pp. 1776–1784. doi:10.2514/3.1924

[15] Goulard, R., "On Catalytic Recombination Rates in Hypersonic Stagnation Heat Transfer," *Jet Propulsion*, Vol. 28, 1958, pp. 737–745.

[16] Scott, C. D., "Recombination of Atomic Species on Surfaces," *Molecular Physics and Hypersonic Flows*, edited by M. Capitelli, Kluwer, Dordrecht, The Netherlands, 1996.

[17] Blottner, F., "Finite Difference Methods of Solution of the Boundary Layer Equations," *AIAA Journal*, Vol. 8, No. 2, 1970, pp. 193–205. doi:10.2514/3.5642

[18] Barbante, P. F., and Degrez, G., "An Efficient Euler/Navier–Stokes Solver for Reacting Flows," *16th IMACS World Congress 2000* [CD-ROM], Ecole Polytechnique Federale de Lausanne, Lausanne, Switzerland, 21–25 Aug. 2000.

[19] Barbante, P. F., "Accurate and Efficient Modeling of High Temperature Nonequilibrium Air Flows," Ph.D. Thesis, Univ. Libre de Bruxelles, Bruxelles, Belgium, 2001.

[20] Coquel, F., and Liou, M. S., "Hybrid Upwind Splitting Scheme by a Field by Field Decomposition," NASA TM 106843, Jan. 1995.

[21] Hirsch, C., *Numerical Computation of Internal and External Flows*, Vol. 2, Wiley, Chichester, England, U.K., 1990.

[22] Bottin, B., Vanden Abeele, D., Carbonaro, M., Degrez, G., and Sarma, G. S. R., "Thermodynamic and Transport Properties for Inductive Plasma Modeling," *Journal of Thermophysics and Heat Transfer*,

Vol. 13, No. 3, 1999, pp. 343–350.
doi:10.2514/2.6444

[23] Barbante, P. F., "How Diffusion Modeling Affects Prediction of Heat FLux Loads," *Sixth European Symposium on Aerothermodynamics of Space Vehicles*, SP-659, ESA, Noordwijk, The Netherlands, 3–6 Nov. 2008, p. 14-1.

[24] Sutton, K., and Gnoffo, P., "Multi-Component Diffusion with Application to Computational Aerothermodynamics," 7th AIAA/ASME Joint Thermophysics and Heat Transfer Conference, AIAA Paper 98-2575, 15–18 June 1998.

[25] Kolesnikov, A. F., "Combined Measurements and Computations of High Enthalpy and Plasma Flows for Determination of TPM Surface Catalycity," *Measurement Techniques for High Temperature and Plasma Flows*, edited by J. M. Charbonnier and G. S. R. Sarma, NATO Research and Technology Organization, Neuilly-sur-Seine, France, 1999.

[26] Bottin, B., Chazot, O., Carbonaro, M., Van Der Haegen, V., and Paris, S., "The VKI Plasmatron Characteristics and Performance," *Measurement Techniques for High Temperature and Plasma Flows*, edited by J. M. Charbonnier and G. S. R. Sarma, NATO Research and Technology Organization, Neuilly-sur-Seine, France,1999.

[27] Vera, I., and Chazot, O., "Assessment of Pressure and Enthalpy Rebuilding for Simulation of Planetary Re-Entry Conditions in Plasmatron Facility," von Karman Inst., TR SR 2004-37, Rhode-St-Genèse, Belgium, 2004.

[28] Bertin, J. J., *Hypersonic Aerothermodynamics*, AIAA, Washington, D.C., 1994, Chap. 6.

[29] White, F. M., *Fluid Mechanics*, 4th ed., McGraw–Hill, New York, 1998, Chap. 5.

[30] Fletcher, D. G., and Playez, M., "Characterization of Supersonic and Subsonic Plasma Flows," AIAA Paper 2006-3294, 2006.